中國機械工程學刊第四十二卷第三期第 275~284 頁(民國一百一十年)
Journal of the Chinese Society of Mechanical Engineers, Vol.42, No.3, pp 275~284 (2021)

Advanced Control of Hydraulic System for Hydrostatic Bearings

Kai-Chieh Chuang*, Shao-Yang Wang*, Yu-Lun Chiang*
and Jia-Ying Tu**

Keywords: Hydrostatic bearing, restrictor, hydraulic system, model matching control, OFCIA

ABSTRACT

Recent developments in precision manufacturing heighten the need of hydrostatic bearings for machine tools, because of the advantages of high stiffness, high precision, low friction and long service life, as compared with the traditional roller bearing systems. In literature, attention has been paid to the design of fixed-type restrictors such as capillaries for hydrostatic bearings. However, such passive flow restrictors could not effectively compensate for oil pressure variation as a result of loading changes. To seek an alternative for improving the operation precision of hydrostatic bearings, pressure control using active proportional valve is considered in this work. Four proportional valves are installed in the hydraulic system and controlled by advanced output feedback control with integral action and model matching techniques. Experimental studies on the actively-controlled hydrostatic system are performed. The results show that the rising time and tracking accuracy of the oil pressure are effectively improved by the proposed active control framework, thus sustaining the performance of hydraulic bearing. The success of this research offers a feasible control framework for the development of intelligent control and manufacture of machine tools in future work.

INTRODUCTION

High-level manufacturing precision of machine tools is significantly demanded in the mechanical industry. The traditional ball bearing systems that inevitably cause friction, vibration and heat usually degrade high-quality machining. Hydrostatic bearing systems gradually replace ball bearings and become the main components of high-precision machine tools in the last decades because of the advantages of low friction, high stiffness and high accuracy (Lin, 2016). Typically, a hydrostatic bearing includes the main units of bearings, restrictors, recesses and hydraulic system, as shown in Fig. 1. The hydraulic system supplies oil to the recesses of the bearing through the oil pipes and restrictors, and each restrictor is constituted of a capillary. Thus, the restrictor outputs high-pressure oil that allows the recess to generate a high-stiffness oil film to afford and smooth the bearing motion. However, during the operation process, unwanted external loading imposing on the bearing may cause vibration and affect the oil-film thickness. Therefore, to sustain the even thickness and stiffness of the high-pressure oil film via advanced compensation technique is the key to the success of hydrostatic bearing systems.

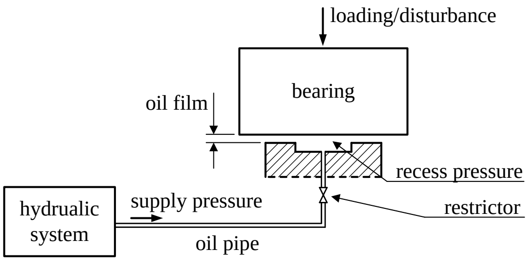

Fig. 1. Scheme and operation of a hydrostatic bearing system.

In literature, many pressure compensation strategies have been developed for hydrostatic bearing systems to maintain the oil-film thickness and stiffness(Pso, 2016). The common strategies are to examine the configuration of the bearing system and to improve the design of fixed-type restrictor by modifying the geometry and flow resistance. As an example, Sharma discussed the optimal number of the

Paper Received July, 2020. Revised Sepfember, 2020. Accepted October, 2020. Author for Correspondence: Kai-Chieh Chuang.

* *Gradnate Student, Department of Power Mechanical Engineering, National Tsing Hua University, Hsinchu, Taiwan 300044, ROC.*

** *Associate Professor, Department of Power Mechanical Engineering, National Tsing Hua University, Hsinchu, Taiwan 300044, ROC.*

capillary restrictors using the finite-element method (Sharma, Jain, Sinhasan, & Shalia, 1995). The results indicated that the bearings with six recesses provided with the best stability and stiffness for the hydrostatic journal bearing. Ling theoretically studied the method of stiffness optimization the using external pressurized bearings. The maximum stiffness of the bearing could be obtained by proper selection of the ratio of the recess pressure to the supply pressure. The ratio was determined by the restrictor constant rather than the film thickness (Ling, 1962).

However, the fixed-type restrictors including unchangeable parameters are unable to accommodate with pressure variations in the face of unexpected loading (W. B. Rowe, 2012). In this aspect, variable-type restrictors with better strength to compensate for oil pressure changes are widely considered in literature. Kang determined the membrane deflection and film thickness of the membrane-type restrictors by FEM (Kang, Shen, Chen, Chang, & Lee, 2007). For example, the membrane-type restrictors (W. Rowe & JP, 1970), which use active membranes to replace capillary, can automatically react to the loading variation and compensate for the hydraulic pressure in a certain range of operation. Moris presented a comparison of the film stiffness and power requirements for actively and passively compensated hydrostatic bearings (Morsi, 1972). Moshin demonstrated that the oil film stiffness generated by the membrane-type restrictors performed better than that by the fixed-type ones (Mohsin, 1963). In addition, Tully reported a novel form of diaphragm restrictor, which offered high stiffness and acted as a vibration absorber to suppress the disturbance due to the dynamic loading (Tully, 1977).

Despite of the benefit of variable-type restrictors, the performance is still constrained by the geometric specification of the restrictors, which may not be able to achieve real-time and wide-range compensation and is not advantageous to further development on intelligent manufacturing. Therefore, the active techniques for pressure regulation are proposed in literature, such as the use and control of spool valves, proportional valves and servo valves (W. B. Rowe, 2012). In the presence of unwanted external disturbance, Shih established an active control technology with servo valves to adjust the oil film thickness (Shih & Shie, 2013). Yang et al. studied the pump-displacement-controlled actuator based on a proportional-integral algorithm combined with feed-forward compensation to realize higher dynamic response and tracking accuracy of the pump-displacement-controlled actuator (Song, Wang, Ren, Cai, & Jing, 2017).

Resting on the previous studies on restrictor design, the purpose of this paper is to examine an active pressure compensation framework for hydrostatic bearing system, based on the use of proportional valves and advanced control methods. To this end, a multi-input/multi-output hydraulic system equipped with four proportional valves is developed and presented in the subsequent section. Then, the dual-loop control techniques using PID, output feedback control with integral action and model matching methods are introduced. Experimental work for identifying the parameters and models of the hydraulic system is implemented. The obtained mathematical models provide a base for *a priori* simulation studies on control design and performance evaluation. Finally, experimental results of different control cases are compared, in order to verify the effectiveness and robustness of the proposed pressure compensation techniques.

DEVELOPMENT OF ACTIVE-CONTROL HYDROSTATIC SYSTEM

In this section, the design and control scheme of the active hydraulic system is introduced.

Fig. 2 draws the oil loop of the hydraulic system, including the major components of a pump, four proportional pressure valves, five pressure sensors, a relief valve, a filter, an accumulator, an oil return motor etc. As shown in

Fig. 2, the oil pumped up from the oil tank passes through the proportional pressure valves and restrictors, and the oil block is used to connect the restrictors with pressure valves. The outputs of restrictors are recesses, which generate high-pressure and high-stiffness oil film to afford the bearing components. Meanwhile, the relief valve and an oil return motor regulate the unneeded oil flow back to the oil tank. Considering the required oil pressure and power capacity, the specification of the pump is selected to be 5 H power. In addition, between the pump and the pressure valves, the oil pipe is equipped with a filter for reducing the impurities in the oil flow. For safety reason, an accumulator is connected to the oil pipe to maintain the oil pressure for a period of time in the presence of unexpected power off.

Referring to

Fig. 2, an experimental rig is developed in

Fig. 3. Four pressure sensors are installed between the pressure valves and the restrictors to measure the real-time pressure signals. Therefore, the pressures valves along with the pressure sensors construct four active control loops, where the input voltage of the pressure valve are denoted as u_{i1}, u_{i2}, u_{i3} and u_{i4}, respectively, and the measured pressure signals are written as y_1, y_2, y_3 and y_4, respectively. Each proportional pressure valve operates at the range of 0-10 V, the compatible pressure output is 10-50 bar, and the measurement range of the pressure sensor is 0-100 bar.

Furthermore, the hydraulic system consisting of four active control loops are designed for two possible advanced application purposes. Firstly, each loop is used to control one bearing unit, and thus the hydraulic system is able to operate a maximum of four machine tools simultaneously. Secondly, when a machine tool contains four restrictors, the four control loops can modulate individual oil pressure according to the operation condition as a whole. Thus, with the two application purposes, this research would facilitate the development of intelligent control and multi-functionality for machine tools.

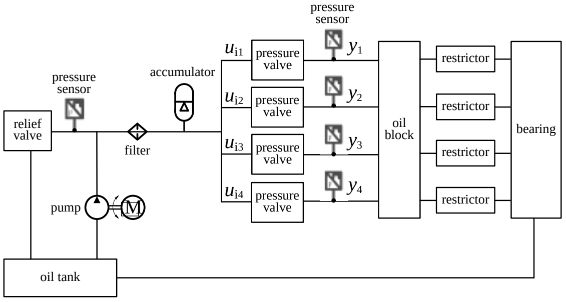

Fig. 2. Design scheme and oil loop of hydraulic system.

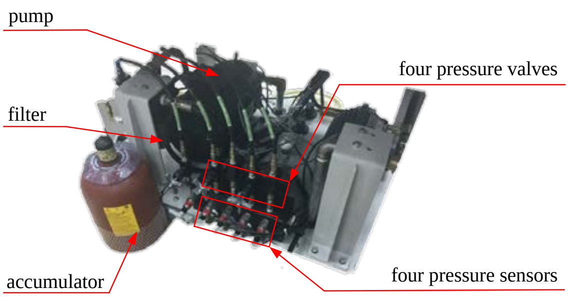

Fig. 3. Experimental rig of hydraulic system.

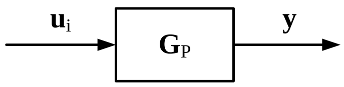

Fig. 4. Input-output block diagram of hydraulic system (Chuang, Chen, & Tu, 2016).

Based on Fig. 2 and Fig. 3, the input-output block diagram of the multi-input/multi-output (MIMO) hydraulic system is drawn in

Fig. 4, where the hydraulic system is denoted as $\mathbf{G}_\mathrm{P}$, and its input and output signals are expressed as vector form, i.e. $\mathbf{u}_\mathrm{i} = [u_{i1}\ u_{i2}\ u_{i3}\ u_{i4}]^T$ and $\mathbf{y} = [y_1\ y_2\ y_3\ y_4]^T$. Therefore, the input-output relation between $\mathbf{u}_\mathrm{i}$ and $\mathbf{y}$ in transfer-function form is written as:

$$\underbrace{\begin{bmatrix} y_1(s) \\ y_2(s) \\ y_3(s) \\ y_4(s) \end{bmatrix}}_{\mathbf{y}} = \underbrace{\begin{bmatrix} G_{\mathrm{P}11}(s) & G_{\mathrm{P}12}(s) & G_{\mathrm{P}13}(s) & G_{\mathrm{P}14}(s) \\ G_{\mathrm{P}21}(s) & G_{\mathrm{P}22}(s) & G_{\mathrm{P}23}(s) & G_{\mathrm{P}24}(s) \\ G_{\mathrm{P}31}(s) & G_{\mathrm{P}32}(s) & G_{\mathrm{P}33}(s) & G_{\mathrm{P}34}(s) \\ G_{\mathrm{P}41}(s) & G_{\mathrm{P}42}(s) & G_{\mathrm{P}43}(s) & G_{\mathrm{P}44}(s) \end{bmatrix}}_{\mathbf{G}_\mathrm{P}} \underbrace{\begin{bmatrix} u_{i1}(s) \\ u_{i2}(s) \\ u_{i3}(s) \\ u_{i4}(s) \end{bmatrix}}_{\mathbf{u}_\mathrm{i}}. \tag{1}$$

Here, $\mathbf{G}_\mathrm{P}$ is represented as a 4×4 transfer-function matrix, because the hydraulic system includes four inputs and four outputs, and $G_{\mathrm{P}jk}(s)$ denotes the transfer function between the j^{th} input and the k^{th} output. Furthermore, from the result of system identification, as will be addressed in the experiment section, the $\mathbf{G}_\mathrm{P}$ dynamics can be divided into the strongly-coupled and weakly-coupled terms. In general, the strongly-coupled parts dominate the system responses, and the effect of weakly-coupled dynamics is almost negligible. Therefore, the off-diagonal elements of $\mathbf{G}_\mathrm{P}$ related to the weakly-coupled dynamics are removed, and that simplifies $\mathbf{G}_\mathrm{P}$ to a diagonal transfer-function matrix:

$$\mathbf{G}_\mathrm{P}(s) = \begin{bmatrix} G_{\mathrm{P}11}(s) & 0 & 0 & 0 \\ 0 & G_{\mathrm{P}22}(s) & 0 & 0 \\ 0 & 0 & G_{\mathrm{P}33}(s) & 0 \\ 0 & 0 & 0 & G_{\mathrm{P}44}(s) \end{bmatrix}. \tag{2}$$

Based on equations (1) and (2), the MIMO system can be decoupled and represented as four single-input/single-output (SISO) plants as follows:

$$y_k(s) = G_{\mathrm{P}kk}(s) u_{ik}(s), \tag{3}$$

where the subscript number j equates to k and k is from one to four. The SISO representation of equation (3) would facilitate the control system design to be developed in a relatively straightforward manner.

Then, the dual-loop control scheme for each SISO plant is drawn in

Fig. 5, which contains an inner loop and an outer loop. Typically, many high-quality, commercialised hydraulic systems are embedded with inner-loop controllers, in order to achieve the high demand on stability and safety, as well as to maintain the fundamental control performance. Such a proprietary controller is usually tailored by the PID algorithm. Similarly, in our case of

Fig. 5, the inner-loop PID controller for $G_{\mathrm{P}kk}$ is developed and is denoted as G_{ik}, while the design is not discussed herein for brevity.

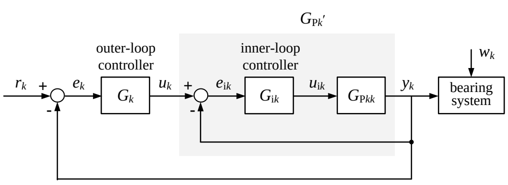

Fig. 5. Dual-loop control of the hydrostatic bearing system.

Nevertheless, in many situations, the inner-loop PID controller may not be good enough to guarantee robust tracking of y_k in the presence of unexpected loading variation or disturbance, which is collectively represented as w_k in

Fig. 5. The disturbance acting on the hydrostatic bearing may have high-frequency and large-amplitude characteristics, incurring unwanted vibration and degrading the oil film stiffness. Thus, an advanced outer-loop controller, written as G_k, would be required to enhance the tracking robustness. As shown in

Fig. 5, the G_k controller computes an outer-loop control signal, represented as u_k, and r_k denotes the reference signal (designated pressure). Therefore, u_k, y_k and r_k constitute an outer-loop, closed-loop system. Under the dual-loop scheme, u_k is taken as the reference signal of the G_{ik} controller, and G_{ik} together with the G_{Pkk} dynamics are viewed as a new plant, expressed as:

$$G_{Pk}'(s) = \frac{y_k(s)}{u_k(s)} = \frac{G_{ik}(s)G_{Pkk}(s)}{1+G_{ik}(s)G_{Pkk}(s)} . \tag{4}$$

As shown in equation (4) and

Fig. 5, the closed-loop dynamics including G_{ik} and G_{Pkk} is considered as a new plant, denoted as G_{Pk}'. In this manner, the tracking error dynamics with respect to the inner-loop and outer-loop yield:

$$e_{ik}(s) = u_k(s) - y_k(s) = u_k(s) - G_{Pkk}(s)u_{ik}(s) , \tag{5}$$

$$e_k(s) = r_k(s) - y_k(s) = r_k(s) - G_{Pk}'(s)u_k(s) , \tag{6}$$

where e_{ik} and e_k denote the inner-loop and outer-loop tracking errors, respectively. It is noted again that, the subscript number k is from one to four, representing the SISO error signal of the hydraulic system. Accordingly, the G_{ik} controller is designed using the PID technique, and the G_k controller is addressed in the subsequent section.

DEVELOPMENT OF OUTER-LOOP CONTROL ALGORITHMS

The structure of dual-loop control scheme has been introduced in in the previous section, and the control object of outer-loop controller is to regulate e_k to approach zero in a stable, fast and robust manner, despite of w_k. To this end, the advanced control algorithms of output feedback control with integral action and model matching method are introduced in this section. It is to be noted that, because the MIMO plant has been decoupled to four SISO systems, the control design is conducted based on the SISO scheme referring to

Fig. 5, without the loss of generality. Thus, in the following description, the subscript number k represents the k^{th} control loop of the hydraulic system, and k is from one to four.

Output feedback control with integral action

The first control technique of output feedback control with integral action (OFCIA) is introduced with reference to (Chen, 1999), and the control block diagram is drawn in Fig. 6. The design of OFCIA includes a state-feedback and an integral controller, and the integral gain ensures zero steady-state error, despite parameter variations and noises around the system. Referring to equation (4), the state-space realisation of G_{Pk}' is assumed to be:

$$\dot{\mathbf{x}}_k(t) = \mathbf{A}_k \mathbf{x}_k(t) + \mathbf{B}_k u_k(t) , \tag{7}$$

$$y_k(t) = \mathbf{C}_k \mathbf{x}_k(t) , \tag{8}$$

where $\mathbf{A}_k$, $\mathbf{B}_k$ and $\mathbf{C}_k$ correspond to the plant, input and output matrices, and $\mathbf{x}_k$ is the state vector. Here, the state variables within $\mathbf{x}_k$ are assumed to be fully measurable, and thus the control law of OFCIA is proposed as:

$$u_k = -\mathbf{K}_k \mathbf{x}_k + K_{Ik} x_{Ik} , \tag{9}$$

where $\mathbf{K}_k$ is the state feedback gain matrix for promoting the stability and transient response, and K_{Ik} is the integral gain for reducing the tracking error in steady state. In addition, x_{Ik} is defined as the integral of tracking error between r_k and y_k as follows

$$x_{Ik} = \int_0^t e_k \,\mathrm{d}\tau = \int_0^t (r_k - y_k)\,\mathrm{d}\tau . \tag{10}$$

With the substitution of equation (9) into (7), the closed-loop dynamics yields:

$$\dot{\mathbf{x}}_k = \left(\mathbf{A}_k - \mathbf{B}_k \mathbf{K}_k\right)\mathbf{x}_k + \mathbf{B}_k K_{Ik} x_{Ik} . \tag{11}$$

Therefore, the pole placement technique can be used to synthesise $\mathbf{K}_k$ and K_{Ik}. Moreover, in the case that the state variables in $\mathbf{x}_k$ are not fully measurable, a state observer (Chen, 1999) is used to estimate the states as follows:

$$\dot{\hat{\mathbf{x}}}_k = \left(\mathbf{A}_k - L_k \mathbf{C}_k\right)\hat{\mathbf{x}}_k + \mathbf{B}_k u_k + L_k y_k . \tag{12}$$

In equation (12), the estimated state vector is denoted as $\hat{\mathbf{x}}_k$, to be distinguish from $\mathbf{x}_k$, and L_k is the observer gain matrix. Thus, the stability of the observer is governed by the eigenvalues of ($\mathbf{A}_k - L_k\mathbf{C}_k$). Typically, in order to enhance the system performance, it is required that the eigenvalues of the observer are faster than those of the state feedback controller.

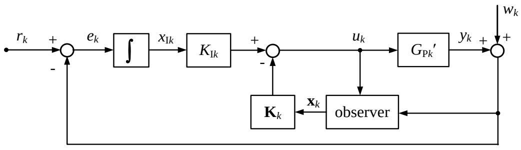

Fig. 6. Block diagram of output feedback control with integral action.

Model matching method

For a better comparison of the control performance, the second controller of model matching (MM) method is considered (Chen, 1999), and

Fig. 7 shows the control block diagram. In comparison with OFCIA, the MM method allows the desired poles and zeros to be specified intuitively in a reference model, while OFCIA mainly focuses on the technique of pole placement. As shown in

Fig. 7, the first step of the MM method is to design an ideal reference model with the designated performance and specification, where the reference model is denoted as G_{rk}, and its input-output transfer function is given by:

$$G_{rk}(s) = \frac{y_{rk}(s)}{r_k(s)} = \frac{N_{rk}(s)}{D_{rk}(s)}, \tag{13}$$

where D_{rk} and N_{rk} are the denominator and numerator of G_{rk}, respectively, and y_{rk} is the output of G_{rk}. Then, referring to equation (4), the expression for G_{Pk}' is re-written as:

$$G_{Pk}'(s) = \frac{y_k(s)}{u_k(s)} = \frac{N_k(s)}{D_k(s)}, \tag{14}$$

where D_k and N_k are the denominator and numerator, respectively, and they are assumed to be coprime polynomials. Therefore, to enable the closed-loop system of G_{Pk}' to behave like G_{rk}, the MM controller is proposed to shape the loop gain, which includes a feedforward and a feedback compensator as follows:

$$u_k(s) = -C_{yk}(s)y_k(s) + C_{rk}(s)r_k(s), \tag{15}$$

In equation (15), C_{rk} and C_{yk} are the feedforward and feedback component, respectively, and the expression for C_{rk} and C_{yk} are assumed to be:

$$C_{rk}(s) = \frac{P_k(s)}{H_k(s)}, \tag{16}$$

$$C_{yk}(s) = \frac{M_k(s)}{H_k(s)}, \tag{17}$$

where H_k is defined as the common denominator obtained from C_{rk} and C_{yk}, and P_k and M_k are the numerators of C_{rk} and C_{yk}, receptively. With the substitution of equations (16) and (17) into (15), the control equation becomes:

$$u_k(s) = -\frac{M_k(s)}{H_k(s)}y_k(s) + \frac{P_k(s)}{H_k(s)}r_k(s). \tag{18}$$

Then, substituting equation (18) into (14), the input and output dynamics are re-arranged and yield the following closed-loop transfer function:

$$\frac{y_k(s)}{r_k(s)} = \frac{N_k(s)P_k(s)}{D_k(s)H_k(s) + N_k(s)M_k(s)}. \tag{19}$$

Finally, comparing equation (19) with (13), the closed-loop transfer function is required to match the reference model, and thus the polynomials coefficients of the controller, including $H_k(s)$, $P_k(s)$ and $M_k(s)$, can be determined.

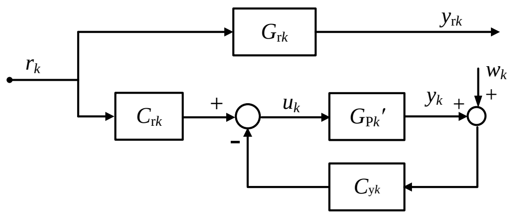

Fig. 7. Block diagram of model matching method.

EXPERIMENT AND CONTROL RESULTS

Based on the results of the previous two sections, the system identification for the experimental rig of

Fig. 3 is carried out first to obtain the parameters and transformed models of the hydraulic system. The obtained models are used for dynamic simulation and control synthesis. Then, a series of tests are conducted to validate the performance of the hydraulic system and controllers. Herein, all the experiment was implemented using the dSPACE control system, and both the control and data sampling intervals were set to be 0.001 s. The inner-loop PID gains for each proportional pressure valve in

Fig. 3 were selected to be k_p = 0.07, k_i = 1.0 and k_d = 0.005 ultimately, after an iterative and empirical adjustment.

System identification

Two different excitations were sent to the hydraulic system for identifying the G_{Pk}' models of equation (4), i.e. square and swept sinusoidal signals, and the y_1, y_2, y_3 and y_4 were measured. With referring to

Fig. 5, the input signal u_1 and the measured output y_1 are presented in

Fig. 8 to identify G_{P1}', as an example of demonstration, while the other identification results are not shown for brevity. In

Fig. 8, u_1 and y_1 are plotted using black-dotted and black-solid line, respectively. Here, u_1 is a swept sine wave with an amplitude of 1 bar and frequencies ranging from 0.1 Hz to 1 Hz. Here, a preload of 20 bar is required in order to initiate the hydraulic system and to generate the oil film.

Fig. 8 indicates that the amplitude of y_1 is smaller than that of u_1 and the amplitude difference gradually increases with the frequency.

The recorded input and output data of u_1 and y_1 were analysed using the Matlab *oe* function. Table 1 shows the identified transformed model of G_{P1}' in nominal condition, and

Fig. 9 presents its frequency-dependent dynamics using Bode diagram. Table 1 and

Fig. 9 show that the pole, low-frequency gain, and rise time of G_{P1}' are -4.29, 4.17 dB, and 0.51 s, respectively. The result, indicates a relatively sensitive and slow-response system because the pole is close to the imaginary axis. Similarly, the same approach is applied to identify G_{P2}', G_{P3}' and G_{P4}', and the obtained models are summarised in Table 1. As shown in Table 1, although the MIMO hydraulic system is decoupled to four SISO control loops, the four SISO plant dynamics are very similar. Four SISO control loops with similar models are advantageous for decoupled control, because the ill-conditioned (coupled) dynamics due to different models may incur control design difficulty.

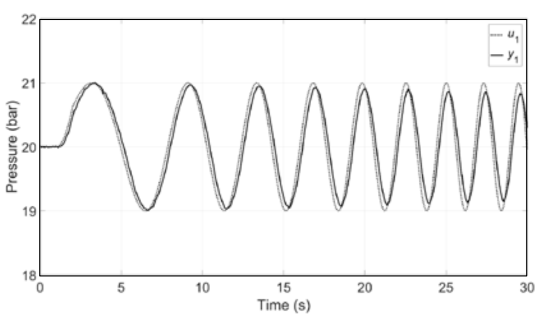

Fig. 8. Relationship between input signal and measure output.

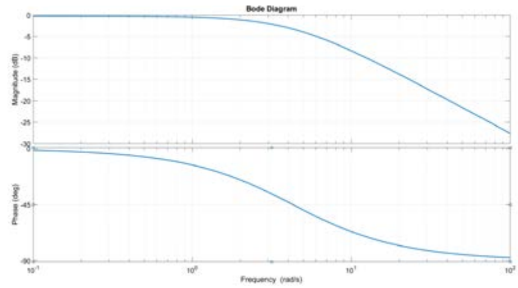

Fig. 9. Bode diagram of G_{11}'.

Control synthesis

The nominal models in Table 1 provide with a foundation for the design and synthesis of control gains, and only the first SISO control loop is discussed in the following for brevity. With reference to equations (9)-(12),the first step of OFCIA design to transform the transfer function of G_{P1}' into state-space model as follows:

$$\mathbf{A}_1 = -20\,,\ \ \mathbf{B}_1 = 1\,,\ \ \mathbf{C}_1 = 20\,. \tag{20}$$

To increase the settling time and improve the stability, the control and observer gain matrices are determined as:

$$\mathbf{K}_1 = 10\,,\ K_{I1} = 6.5\,,\ L_1 = 7.7\,, \tag{21}$$

which moves the closed-pole from -4.29 to -20, such that the settle time is promoted from 0.912 to 0.1 s. The observer pole is assigned to be faster than the OFCIA pole, which are located at 44. The OFCIA gains for the other three loops are synthesized with the same specification, and the results are addressed presented in Table 1. In terms of the MM control synthesis, referring to equation (13) and the G_{P1}' dynamics, the ideal reference model of G_{r1} is selected to be:

$$G_{r1} = \frac{20}{s+20}\,. \tag{22}$$

The designated specification is meant to increase the rising time of the hydraulic system from 0.51 to 0.11 s. Given the G_{r1} model and referring to the design procedure in equations (15)-(19), the feedforward compensator, C_{r1}, and the feedback compensator, C_{y1}, are synthesized below:

$$C_{r1}(s) = \frac{2s+10}{s+10}\,. \tag{23}$$

$$C_{y1}(s) = \frac{0.75s}{s+10}\,. \tag{24}$$

Then, the MM controllers for the other three SISO control loops are synthesised following the same procedure, and the results are summarised in Table 1.

Table 1. System identification results and control gain synthesis.

	plant transfer function	OFCIA method	MM method
first loop (u_1 and y_1)	$G_{P1}' = \frac{4.17}{s+4.29}$	$\mathbf{K}_1 = 10$ $K_{I1} = 6.5$ $L_1 = 7.7$	$G_{r1} = \frac{20}{s+20}$ $C_{r1}(s) = \frac{2s+10}{s+10}$ $C_{y1}(s) = \frac{0.75s}{s+10}$
second loop (u_2 and y_2)	$G_{P2}' = \frac{4.51}{s+4.68}$	$\mathbf{K}_2 = 23.5$ $K_{I2} = 2.175$ $L_2 = 1.175$	$G_{r2} = \frac{20}{s+20}$ $C_{r2}(s) = \frac{4.4s+8.9}{s+8.5}$ $C_{y2}(s) = \frac{1.95s}{s+8.5}$
third loop (u_3 and y_3)	$G_{P3}' = \frac{4.68}{s+4.87}$	$\mathbf{K}_3 = 23.5$ $K_{I3} = 2.175$ $L_3 = 1.175$	$G_{r3} = \frac{20}{s+20}$ $C_{r3}(s) = \frac{4.3s+8.5}{s+8.2}$ $C_{y3}(s) = \frac{1.91s}{s+8.2}$
fourth loop (u_4 and y_4)	$G_{P4}' = \frac{4.93}{s+5.31}$	$\mathbf{K}_4 = 35$ $K_{I4} = 35$ $L_4 = 7.7$	$G_{r4} = \frac{20}{s+20}$ $C_{r4}(s) = \frac{4.1s+8.1}{s+7.5}$ $C_{y4}(s) = \frac{1.86s}{s+7.5}$

Implementation results

In this subsection, the results of control implementation of the hydraulic system are shown. The experiment work are dividied in two parts. Firstly,

Fig. 10 and

Fig. 11 show the experimental results of the OFCIA and MM method,respectively, and their control performance are compared. On the left-hand side of the two figures, the dotted and the solid lines are the reference and the measured output signals, respectively. The outer-loop control signals are shown in the right-hand side column.

Fig. 10 shows that when the magnitude of reference signal changes, the control signals result in significant peaks, while the peak phenomenon is unseen in

Fig. 11. In addition, OFCIA yields better tracking accuacy in the transit state than that of the MM method. The tracking inaccurance and the peak control signal is resulted by the mathematical principles of the MM method.

Fig. 12 uses the first SISO control loop as an example to show the necessity of the outer-loop control strategy. The experimental results of inner-loop PID controller, OFCIA controller, and MM controller are shown in

Fig. 12 (a),

Fig. 12 (b), and

Fig. 12 (c), respectively. The dotted and the solid lines are the reference and the measured output signals, respectively. The experimental results of only using the inner-loop PID controller are compared to those of adding an outer-loop controller. The control comparsion are characterised and quantified in Table 2. The rise time and setting time under the inner-loop PID control are 0.512 and 0.912 s, respectively. The rise time and setting time of the MM method are 0.098 and 0.187 s. The rise time and setting time of the OFCIA are 0.054 and 0.1 s. Accordingly, the addition of outer-loop controller reduces the rising time and setting time, effectively. And the OFCIA method obtains the best performance characteristics.

In the final part of implementation work, the robustness of controller is discussed. From the above experimental results, the dual-loop control using OFCIA yields the best performance. In order ot verify the roubustness of the controller, a hydrostatic bearing (Shiu, 2019) is connected to the oil block of the hydraulic system. In words, the hydraulic system of

Fig. 2 is connected to the bearing system in

Fig. 13. The supply oil pressure was set to be 20 bar and the test time was set to be 30 s. Then, the load on the hydrostatic bearing was increased with an increment of 1kg until 2kg. The results of OFCIA controller with loading are shown in

Fig. 14. The experimental results of OFCIA under noload, a load of 1 kg, and a load of 2 kg are shown in

Fig. 14 (a),

Fig. 14 (b), and

Fig. 14(c), respectively. From

Fig. 14, the OFCIA controller could be performed when the hydrostatic bearing encounters external load.

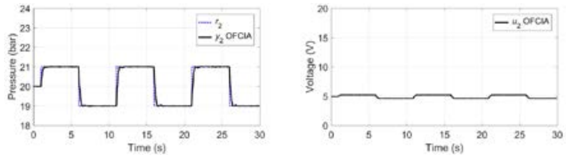

(a) Experimental result of y_2

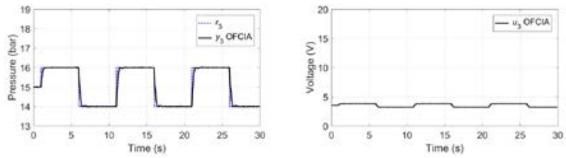

(b) Experimental result of y_3

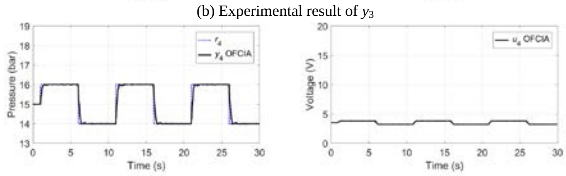

(c) Experimental result of y_4

Fig. 10. Experimental results with OFCIA method.

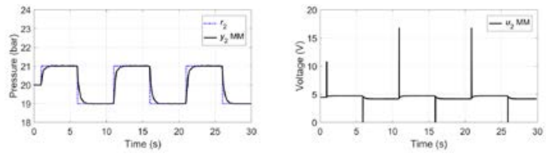

(a) Experimental result of y_2

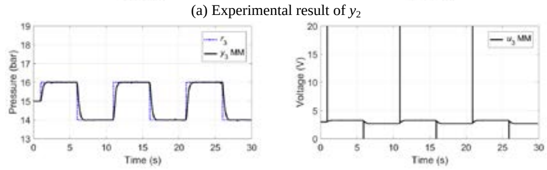

(b) Experimental result of y_3

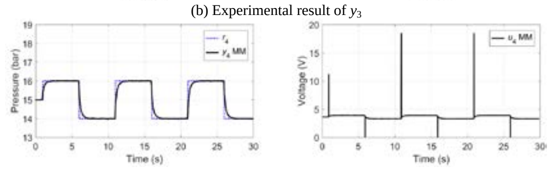

(c) Experimental result of y_4

Fig. 11. Experimental results with MM method.

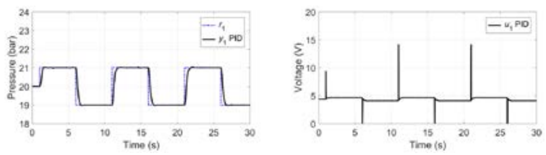

(a) Experimental result of the inner-loop

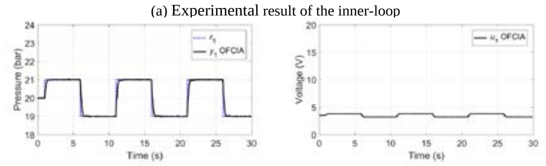

(b) Experimental result of the OFCIA

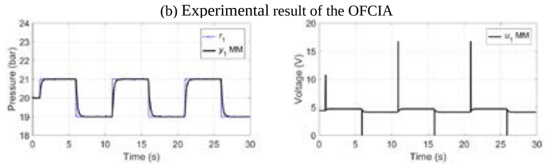

(c) Experimental result of the MM

Fig. 12. Comparison of experimental results between the inner-loop PID controller and outer-loop controller.

Table 2. Summary of performance characteristics using two method.

Methods	Rise time (s)	Setting time (s)
Inner-loop	0.512	0.912
OFCIA	0.054	0.1
Model matching	0.098	0.187

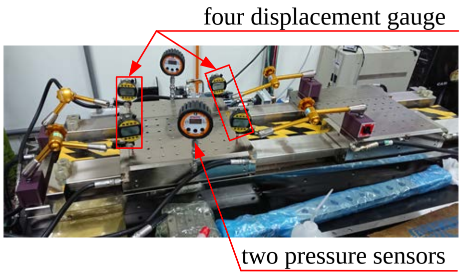

Fig. 13. Experimental rig of hydrostatic bearing (Shiu, 2019).

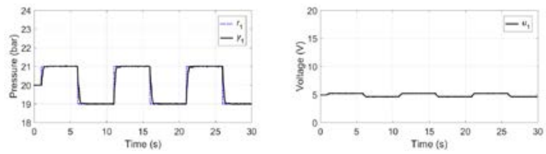

(a) Experimental result under noload

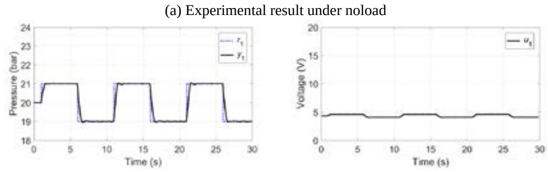

(b) Experimental result under a load of 1 kg

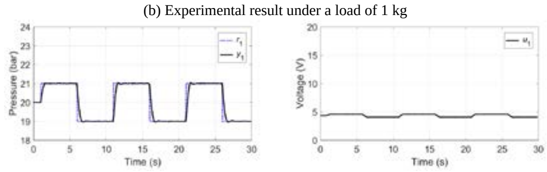

(c) Experimental result under a load of 2 kg

Fig. 14. Experimental result of the OFCIA with loading.

CONCLUSIONS

This paper develops an active hydraulic system for hydrostatic bearing devices with two advanced purposes. First, the hydraulic system can support multiple machine tools simultaneously, and secondly, the oil pressure of different restrictors within a bearing unit can be controlled individually. To this end, four proportional pressure valves are added to the hydraulic system as the active control device for adjusting the oil pressure of the capillary restrictor. In addition, the OFCIA and MM methods are considered to modulate the pressure valves, in order to enhance the response speed and tracking accuracy of the hydraulic pressure. Experimental work of system identification is conducted to identify the transfer functions of the hydraulic system, and a series of testing results show that the proposed controllers are able to adjust the oil pressure, and OFCIA provides the best control performance. The results also indicate that the two advanced function of active hydraulic system is achievable under the current framework, thus offering a base for further development on intelligent control and manufacture of machine tools in near future.

ACKNOWLEDGEMENTS

The authors wish to acknowledge the partial financial support of this study by the HIWIN Technologies Corp., and are also grateful to Prof. C. K. Sung and Prof. S. C. Lin for their supporting.

REFERENCES

Chen, C.-T., Linear System Theory and Design: Oxford University Press, Inc (1999).

Chuang, J.-C., Chen, C.-Y., & Tu, J.-Y.,. "Active Control of Multi-Input Hydraulic Journal Bearing System," Journal of Physics: Conference Series, Volume 744, 13th International Conference on Motion and Vibration Control (MOVIC 2016) and the 12th International Conference on Recent Advances in Structural Dynamics (RASD 2016) 4–6 July 2016, Southampton, UK., 744(1), 012062 (2016).

Kang, Y., Shen, P.-C., Chen, C.-H., Chang, Y.-P., & Lee, H.-H., "Modified determination of fluid resistance for membrane-type restrictors," Industrial Lubrication and Tribology, 59(3), 123-131 (2007).

Lin, Y.-X., A Horizontal Hydrostatic Rotary Bearing Design and Analysis, Master's thesis. (Master Master's thesis), National Tsing Hua Unversity (2016).

Ling, M. T., "On the optimization of the stiffness of externally pressurized bearings," Journal of Basic Engineering, 84(1), 119-122 (1962).

Mohsin, M., "The use of controlled restrictors for compensating hydrostatic bearings," Paper presented at the Proceedings of the third international machine tool design research conference, University of Birmingham (1963).

Morsi, S., "Passively and actively controlled externally pressurized oil-film bearings," Journal of Lubrication Technology, 94(1), 56-63 (1972).

Pso, S.-C., Design of an Intelligent Linear Hydrostatic Slide Module. (Master Master's thesis), National Tsing Hua Unversity (2016).

Rowe, W., & JP, O., "Diaphragm valves for controlling opposed pad hydrostatic bearings," Paper presented at the IndIndustrial Lubrication and Tribology (1970).

Rowe, W. B., "Hydrostatic, Aerostatic, and Hybrid Bearing Design," Elsevier (2012).

Sharma, S. C., Jain, S. C., Sinhasan, R., & Shalia, R., "Comparative study of the performance of six-pocket and four-pocket hydrostatic/hybrid flexible journal bearings," Tribology international, 28(8), 531-539 (1995).

Shih, M. C., & Shie, J. S., "Recess Design and Dynamic Control of an Active Compensating Hydrostatic Bearing," Journal of Advanced Mechanical Design Systems and Manufacturing, 7(4), 706-721. doi:10.1299/jamdsm.7.706 (2013)

Shiu, S.-C., Analysis of Hydrostatic Bearing with Capillary Restrictors, Master's thesis. (Master Master's thesis), National Tsing Hua University (2019).

Song, Y., Wang, D., Ren, H., Cai, J., & Jing, B., "Research on hydraulic pump displacement control using PI and feed-forward compensation," Advances in Mechanical Engineering, 9(12), 1687814017744087 (2017).

Tully, N., "Static and dynamic performance of an infinite stiffness hydrostatic thrust bearing," Trans. ASME, Ser. F, 99, 106 (1977).

NOMENCLATURE

$\mathbf{A}_k$ plant matrix

$\mathbf{B}_k$ input matrix

$\mathbf{C}_k$ output matrix

C_{rk} feedforward compensator of MM controller

C_{yk} feedback compensator of MM controller

D_k denominator polynomial of G_{Pk}'

D_{rk} denominator polynomial of G_{rk}

e_{ik} inner-loop tracking error

e_k outer-loop tracking error

G_{ik} inner-loop controller

G_k outer-loop controller

$\mathbf{G}_P$ transfer function matrix

G_{Pjk} transfer function between the j^{th} input and the k^{th} output

G_{Pk}' inner-loop transfer function including a PID controller

G_{rk} reference model of MM controller

H_k common denominator obtained from C_{rk} and C_{yk}

$\mathbf{K}_k$ state feedback gain matrix

K_{Ik} integral gain

L_k observer gain matrix

P_k numerator polynomial of C_{rk}

M_k numerator polynomial of C_{yk}

N_k numerator polynomial of G_{Pk}'

N_{rk} numerator polynomial of G_{rk}

r_k reference signal of oil pressure

u_{ik} inner-loop control signal

$\mathbf{u}_i$ MIMO inner-loop control signals in vector form

u_k outer-loop control signal

w_k external loading or disturbances

x_{Ik} integral of e_k

$\mathbf{x}_k$ state vector of G_{Pk}'

$\hat{\mathbf{x}}_k$ estimated state vector of G_{Pk}'

$\mathbf{y}$ MIMO measured output signals in vector form

y_k measured output signal

y_{rk} output signal of reference model

液靜壓軸承進階控制

莊鎧榤 王紹陽 江宇倫 杜佳穎
國立清華大學動力機械工程學系

摘 要

近年來液靜壓軸承相較於傳統的滾珠軸承，具有高剛性、高精度、低摩擦和壽命長的優勢，工具機產業著重在液靜壓軸承的發展。在文獻中，液靜壓毛細管節流器的設計被廣泛的探討，然而被動式的裝置無法有效地補償負載造成的油壓變化，本文提出另一種替代的方法，使用主動式比例壓力閥進行壓力控制來提高液靜壓軸承運行的精度。在液靜壓軸承系統中安裝四個比例閥，利用進階輸出反饋控制法和模型匹配法進行控制，並對液靜壓系統進行實驗研究，實驗結果顯示所提出的主動控制架構有效地改善油壓的上升時間和追蹤精度。本文研究結果對未來的智能控制的發展和工具的製造提供一種可行的控制架構。